A unifying model for fluid flow and elastic solid deformation: a novel approach for fluid-structure interaction and wave propagation

S. Bordère[a] and J.-P. Caltagirone[b]

a. *CNRS, Univ. Bordeaux, ICMCB, UPR 9048, F-33600 Pessac, France*
b. *IPB, Univ. Bordeaux, I2M - TREFLE, UMR CNRS 5295, 16 Av. Pey-Berland, 33607 Pessac Cedex, France*

Abstract :

Fluid-structure coupling is addressed through a unified equation system for compressible Newtonian fluid flow and elastic solid deformation. This is done introducing thermodynamics within the Cauchy's equation through isothermal compressibility coefficient. The vectorial resolution of the governing equation, can thus be carried out through a monolithic scheme involving no iterative coupling. For system equation closure, mass density and pressure are both re-actualised from velocity vector divergence, when the shear stress tensor within solid phase is re-actualised from the variation of displacement vectors. This novel approach is first validated on a two-phase system, involving a plane fluid-solid interface, through the two following test cases : i) steady-state compression ; ii) longitudinal and transversal elastic wave propagations. Then the 3D study of a compressive fluid injection towards an elastic solid is analysed from the initial time to the steady-state evolution.

Keywords : fluid-structure interaction, monolithic, elastic wave propagation

1 Introduction

Fluid flow and solid deformation coupling as well as wave propagations are important concerns in many applications in aeronautics [3] and biomedicine [1, 7]. This multi-physics problem involving fluid-solid interfaces can be simulated in a partitioned or monolithic way. In a partitioned approaches [4, 3], fluid and structure equations are resolved sequentially which may result in numerical instabilities due to different time integration schemes for fluid and solid solvers. For monolithic approaches [1, 7], the fluid-solid interaction at the interface is resolved simultaneously using iterative coupling schemes leading to numerical stability but time-consuming calculation. If algorithmic improvements are essential to deal with complex fluid-solid problems, developments of new physical models are of great importance as well. The main objective of this work is thus to proposed a unifying model for the fluid flow and elastic solid deformation. This model is an extension to elastic solid phases of a previous developed one dedicated to compressible multi-phase flows [2].

2 Unified multi-phase compressible model for isothermal conditions

Let consider a multi-phase system involving homogeneous fluids and elastic solids with no mass exchange through the interfaces. At constant temperature and under an applied velocity field $\mathbf{V}$, time derivatives of mass density ρ and pressure p depend on velocity divergence $\nabla \cdot \mathbf{V}$. The time integration of these derivatives, from t^0 to $t = t^0 + dt$, gives the Lagrangian form of mass density and pressure at time t :

$$\rho = \rho^0 \mathrm{e}^{-dt\,\nabla\cdot\mathbf{V}} \qquad p = p^0 - \frac{dt}{\chi_T}\,\nabla\cdot\mathbf{V} \tag{1}$$

where ρ^0 and p^0 are mass density and pressure at time t^0 and where χ_T is the isothermal compressibility coefficient defined from T and p^0. For isothermal conditions, the governing equation of the mechanical problem is the conservation of momentum $\rho\mathbf{V}$ defined through the Cauchy's equation (2).

$$\rho\frac{d\mathbf{V}}{dt} = \nabla\cdot\boldsymbol{\sigma} \tag{2}$$

where $\mathbf{V}$ is the velocity vector and $\boldsymbol{\sigma}$ the stress tensor which can be split up into spherical and non-spherical parts by introducing the pressure p, and the shear stress tensor $\boldsymbol{\tau}$: $\boldsymbol{\sigma} = -p\mathbf{I} + \boldsymbol{\tau}$. For the Newtonian viscous behaviour, $\boldsymbol{\tau}$ is expressed as a function of the shear strain rate tensor depending on the first-order time derivative of the velocity vector $\mathbf{V}$:

$$\boldsymbol{\tau} = 2\mu\ \left(\frac{1}{2}(\nabla\mathbf{V} + \nabla^t\mathbf{V}) - \frac{1}{3}\nabla\cdot\mathbf{V}\,\mathbf{I}\right) \tag{3}$$

where μ is the viscosity coefficient. For isotropic elastic solids, $\boldsymbol{\tau}$ is expressed as a function of the shear strain tensor depending on the first-order time derivative of displacement vector $\mathbf{U}$ in the case of small deformations. For an evolving system, the displacement $\mathbf{U}$ at time t can be rewritten as $\mathbf{U} = \mathbf{U}_0 + \mathbf{V}dt$, where $\mathbf{U}_0$ is the displacement vector at time $t^0 = t - dt$. Then, defining the shear stress tensor $\boldsymbol{\tau}^0$ at time t^0 as a function of the $\mathbf{U}_0$-field, the shear stress tensor $\boldsymbol{\tau}$ at time t can be written as :

$$\boldsymbol{\tau} = \boldsymbol{\tau}^0 + 2\mu_E\ dt\ \left(\frac{1}{2}(\nabla\mathbf{V} + \nabla^t\mathbf{V}) - \frac{1}{3}\nabla\cdot\mathbf{V}\,\mathbf{I}\right) \tag{4}$$

where μ_E is the first Lamé coefficient.

The unified governing equation of the multi-phase system involving compressible Newtonian fluids and isotropic elastic solids is obtained from the Cauchy's equation (2) expressed with pressure and shear stress tensor and within which : i) the shear stress tensor of viscous fluids Eq. (3) and elastic solids Eq. (4) are explicited at time t through a unique formulation by introducing the coefficient $\mu*$ ($\mu^* = \mu$ for the viscous fluid and $\mu^* = dt\mu_E$ for the isotropic elastic solid), and the residual shear stress tensor $\boldsymbol{\tau}^0$ (equals zero for viscous fluids) ; ii) the pressure at time t is predicted using the Lagrangian formulation previously defined in Eq. (1) ; iii) only mass density ρ^0 remains defined at time t^0.

$$\rho^0\ \frac{d\mathbf{V}}{dt} = -\nabla\left(p^0 - \frac{dt}{\chi_T}\,\nabla\cdot\mathbf{V}\right) + \nabla\cdot\boldsymbol{\tau}^0 + \nabla\left(\mu^*\left(\nabla\mathbf{V} + \nabla^t\mathbf{V} - \frac{2}{3}\nabla\cdot\mathbf{V}\,\mathbf{I}\right)\right) \tag{5}$$

The unknown variables (p, ρ, $\boldsymbol{\tau}$) are then explicitly determined from velocity vectors and divergences using Eq. (1) and Eq. (4). The coefficients (χ_T, μ^*) are re-actualized from the updating pressure p.

Up to now, velocity, pressure, mass density and shear stress tensor are solved within a Lagrangian formulation. Subsequently, these variables are advected from the total derivatives for the Eulerian resolution as :

$$\frac{\partial X}{\partial t} = \frac{dX}{dt} - \mathbf{V}\cdot\nabla X \tag{6}$$

where $X = V_i,\ p,\ \rho,\ \tau_{ij}$.

3 Numerical method and discretisation

The unified governing equation (Eq. (5)) is discretized in time and space by an implicit volume method on a staggered mesh. For 3D simulations, an iterative bi-conjugate gradient stabilized BICG-StabII, preconditioned under a Modified and Incomplete LU method was implemented. The spatial discretizations employed centred schemes. The elastic solid and fluid phases are numerically built using a phase function C varying within the interval $[0, 1]$. The value of the phase function C is 1

in the elastic solid and 0 in the fluid. The interface between the elastic solid and the fluid is defined as $C = 0.5$. Every point of the system where $C \leq 0.5$ belongs to the fluid and those where $C > 0.5$ belongs to the elastic solid. The phase function is built and at each time advected Eq. (6), like the other variables, using a Volume of Fluid method [6].

4 Test cases and 3D complex simulation

Validation tests were performed by considering a cubic cavity of length side $L = 1$ m containing the fluid and the elastic solid at initial pressure p_i and mass density ρ_i. Compressions are simulated by injecting fluid at a velocity V_0 through the lower cavity surface (Fig. 1a). Velocity field is constraint to zero value at the upper surface of the cavity, and to symmetric conditions at the four lateral surfaces. For the simulation of simple shear deformation, it is the upper surface which is displaced with a velocity V_0 collinear to the X-axis (Fig. 1b). Velocity field is constraint to zero at the lower surface, and periodic conditions are set at the four lateral surfaces. Geometry and boundary conditions for the 3D simulation of fluid-elastic solid interaction is presented in Fig. 1c. Here, the fluid is flowing through a canal to enter a larger volume containing the elastic solid. The canal is crossing an obstacle which numerically implies a penalty of the velocity field, $\mathbf{V} = 0$ within the entire one [5]. Velocity field is constraint to zero value at the upper surface and Neumann conditions are set at the four lateral surfaces. The canal dimension of square section is 0.2 m x 0.4 m x 0.2 m and the elastic solid thickness is 0.4 m.

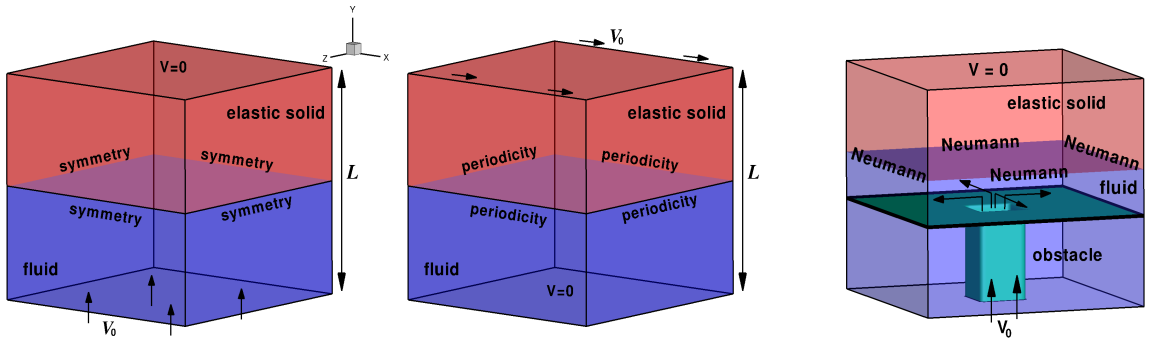

(a) (b) (c)

FIGURE 1 – System geometry and boundary conditions used for the compression (a), the shear deformation (b) and 3D complex problem (c).

The physical characteristics of the phases condidered for both tests cases and complex 3D simulation are : i) for the compressive fluid ; initial mass density $\rho_i = 1.0$ kg.m^3, viscosity coefficient $\mu = 2.0\ 10^{-1}$ Pa.s, isothermal compressibility coefficient $\chi_T = 1.0\ 10^{-5}$ Pa^{-1} and ii) for the elastic solid ; $\rho_i = 1.0$ kg.m^3, Young's modulus $E = 2.0\ 10^3$ Pa, Poisson's coefficient $\nu = 0.4999$. These elastic constants gives a first Lamé's coefficient $\mu_E = 666.7$ Pa, a second Lamé's coefficient $\lambda_E = 3.33\ 10^6$ Pa and an isothermal compressibility coefficient $\chi_T = 3/(2\mu_E + 3\lambda_E) = 3.0\ 10^{-7}$ Pa^{-1}.

4.1 Test case 1 : fluid-elastic solid compression

The 3D simulation of the fluid-elastic solid compression has been carried out on a 11 x 65 x 11 mesh grid using an increment time $\triangle t = 1$ s. During compression, pressure and normalised shear stress defined as $\bar{\boldsymbol{\tau}} = \sqrt{\frac{3}{2}\boldsymbol{\tau} : \boldsymbol{\tau}}$ is verified to be uniform throughout each phase and to evolve linearly with time. Moreover negligible interface displacement is obtained at the final compression time $t_f = 100\ s$. In these above-mentionned conditions, pressure p and shear stress element τ_{yy} within the fluid and elastic solid can be determined analytically and relative errors can thus determined. In Table 1 are shown the calculated values of pressure and normalised shear stress within the two phases for the final compression time. Exact solution is obtained in reference to the low values of relative errors. Pressure and shear stress discontinuities observed at the interface are shown to verified with accuracy

the interface equilibrium criterion (last column of Table 1).

	$p - p_i$ (Pa)	$\frac{p - p_{th}}{p_{th} - p_i}$	$\bar{\tau} - \bar{\tau}_i$ (Pa)	$\frac{\bar{\tau} - \bar{\tau}_{th}}{\bar{\tau}_{th} - \bar{\tau}_i}$	$\tau_{yy} - \tau_{yyi}$ (Pa)	$\tau_{yy}^{(2)} - (p^{(2)} - p^{(1)})n_y$ (Pa)
fluid (1)	1941.763	$2\ 10^{-10}$	0		0	$1.8\ 10^{-7}$
elastic solid (2)	1941.245	$1\ 10^{-8}$	0.776	$2\ 10^{-8}$	-0.518	

TABLE 1 – Pressure and normalised shear stress calculated at the final compression time ; corresponding relative errors and interface quasi-equilibrium criterion.

4.2 Test case 2 : elastic wave propagation

The 3D simulations of elastic wave propagations have been carried out with a 11 x 65 x 11 mesh grid. The propagation of a compression pulse was studied by applying an injection velocity $V_0 = 1.0$ m/s during the first time increment only (Fig. 1). The evolution of pressure during compressive wave propagation is presented in Fig. 2 at two points $M_1(Y_1)$ and $M_2(Y_2)$ along the middle Y-line ($Y_1 = 0.169$ m ; $Y_2 = 0.738$ m).

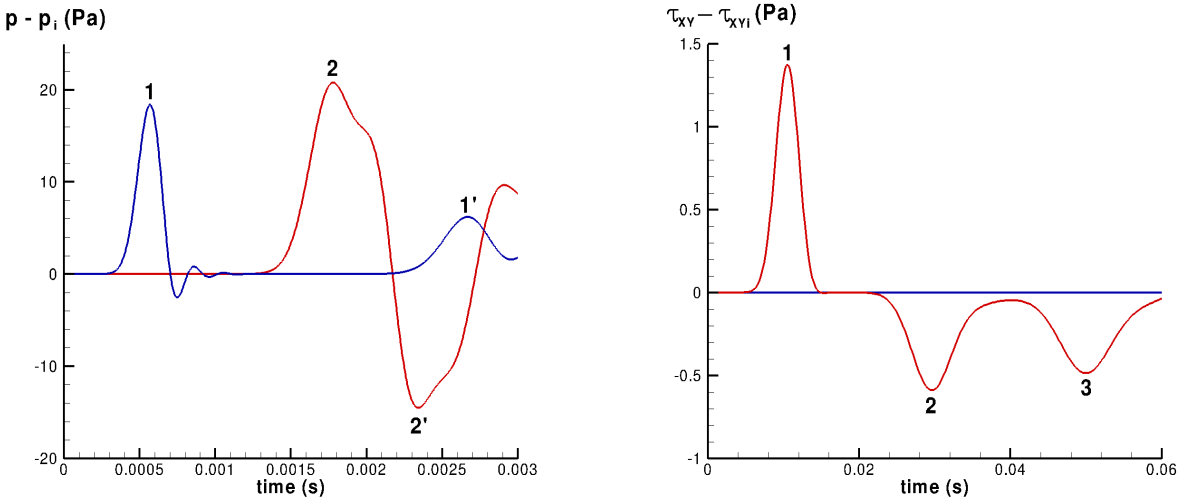

(a) (b)

FIGURE 2 – Pressure evolutions (a) and shear stress evolutions (b) during respectively longitudinal and transversal wave propagations at the M_1- point of the fluid (blue curve) and the M_2- point of the solid (red curve).

The pressure evolution at the M_1-point within the fluid (Fig. 2a) shows two peaks indicated by numbers 1 and 1'. The time interval between these two peaks ($\triangle t_1 = 2.099\ 10^{-3}\ s$) corresponds to the elapse time for the wave to pass at the M_1-point and return to it after interface reflection, and thus to cover the distance $d_1 = 0.662$ m (at the interface the initial wave is split up into two waves, one wave reflecting off the interface and the other one passing through the interface). The pressure evolution at the M_2-point within the solid shows two overlapping compressive peaks (the initial wave passing indicated by number 2 and the first reflected one at the upper surface) followed by two tensile overlapping peaks (major peak indicated by number 2') corresponding to the expansion at the interface of the previous mentioned compression waves. During the time interval between peaks 2 and 2' ($\triangle t_2 = 5.50\ 10^{-4}$ s), the wave covers the distance $d_2 = 1.0\ m$. From the determination of these time intervals and distances, the simulated wave propagation velocities are calculated (see Table 2).

Then, the propagation of a shear deformation pulse was studied by displacing the upper surface of the elastic solid at $V_0 = 1.0\ m/s$ during the first time increment. In Fig. 2b is presented the evolution

of the τ_{xy} element of the shear stress tensor at the M_2-point of the solid. This evolution shows 3 peaks corresponding successively to the initial wave passing, the reversed one after the expansion at the interface and the reflected tensile one. During the time interval between peaks 1 and 3 ($\triangle t_3 = 3.95\ 10^{-2}\ s$) the shear wave covers the distance $d_3 = 1.0$ m allowing the calculation of the shear wave velocity indicated in Table 2. The simulated velocities are shown to be very close to that obtained from theoretical equations (Table 2).

	C_L^{th}(m/s)	C_T^{th} (m/s)	C_L^{cal}(m/s)	C_T^{cal} (m/s)
fluid	316.2	-	315.4	-
elastic solid	1826	25.8	1818	25.3

TABLE 2 – Comparison between theoretical and calculated wave propagation velocities for the two basic cases of longitudinal and transversal wave propagations. For elastic solid, $C_L^{th} = \sqrt{(\lambda_E + 2\mu_E)/\rho}$ and $C_T^{th} = \sqrt{\mu_E/\rho}$; for compressive fluid $C_L^{th} = \sqrt{1/\rho\,\chi_T}$, $C_T^{th} = 0$.

4.3 3D simulation of fluid-elastic solid interaction

The system geometry and boundary conditions are presented in Fig. 1c. The simulation of the fluid injection have been carried out with a 64 x 64 x 64 mesh grid. The injection velocity $V_0 = 15\,\mathrm{m/s}$ is constant during the injection process. The time increment $\triangle t = 5.0\ 10^{-4}$ s is sufficiently low to catch at the beginning of the injection process the pressure fluctuations at the M_2-point of the solid (Fig. 3a) which are time-consistent with the limiting velocity of the longitudinal wave propagation in the fluid (see paragraph 4.2). Other pressure fluctuations are present with a greater order of magnitude of time characteristics. They also characterise the fluid/solid interface movement (Fig. 3b) and they are time consistent with that induced by the propagation velocity of transversal waves in the elastic solid (see paragraph 4.2). These fluctuations of pressure and interface movement reduce gradually with time until the achievement of the steady state of the injection process.

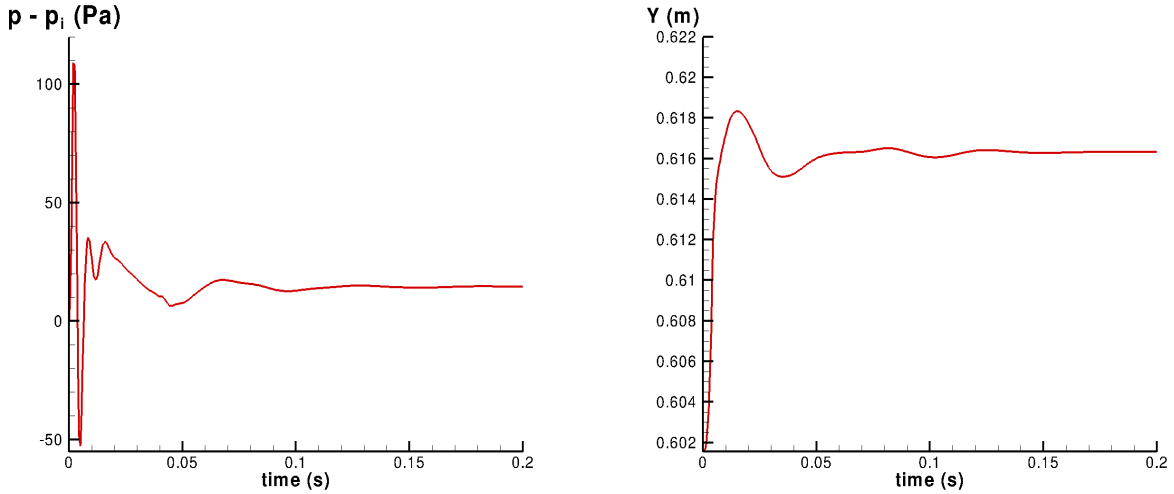

(a) (b)

FIGURE 3 – (a), Evolution of pressure during fluid injection at the M_2-point of the solid ; (b), evolution of the Y-displacement of the middle point of the fluid/solid interface.

The pressure map, streamlines and interface shape during the steady state evolution are shown in Fig. 4a. One can notice that the elastic solid is strictly unmoving as the fluid flows along the interface. The pressure profile along the (X=0.5 ; Y ; Z=0.5)-line (Fig. 4b) exhibits the pressure discontinuity at the interface in consistency with the interface equilibrium condition (see paragraph 4.1).

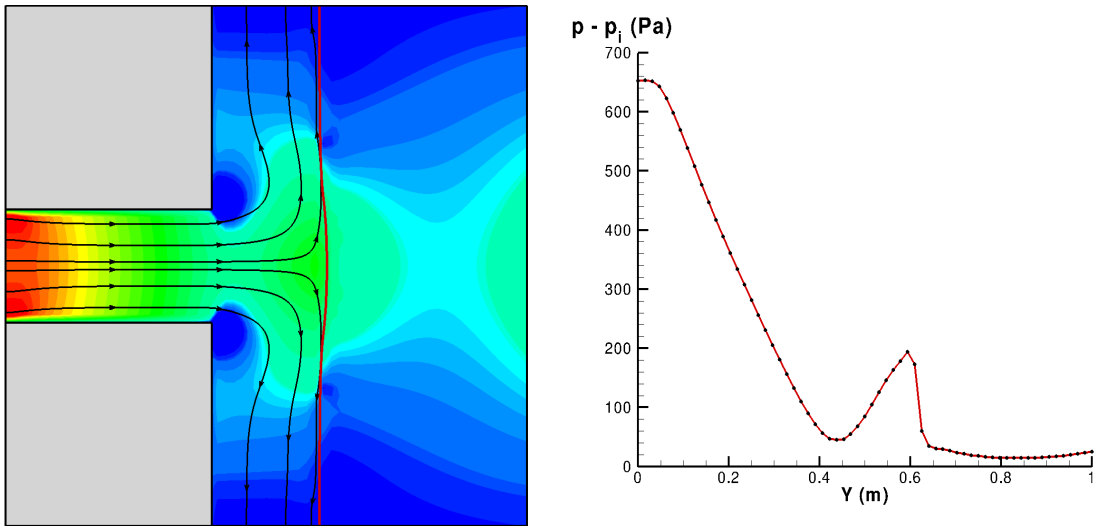

(a) (b)

FIGURE 4 – (a), pressure map (red colour, $p = 700$ Pa ; blue colour $p = 0$ Pa) and streamlines during the steady state evolution ; (b), pressure profile along the (X=0.5, Y, Z=0.5)-line.

5 Conclusion

The main contribution of this work is to have unified, through the same governing equation, the compressible Newtonian viscous flow and the isotropic elastic behaviour. It was mainly done by introducing thermodynamics within the Cauchy's equation, allowing to explicit the compressibility term. Modelling of "incompressible" fluids can thus be carried out with the experimental value of the isothermal compressibility coefficient, without using any additional equation. Moreover, we have to point out that mass density is here no more calculated from the state equation but directly from the velocity divergence value. This unified multi-phase compressible model consequently allows a monolithic vectorial resolution of the governing equation with no iterative coupling. This latter point makes this approach numerically interesting as well. As regards the modelling results, consistent quasi-equilibrium condition at the interface is obtained for the steady state evolution. Non-steady state evolutions can also be studied with accuracy at the time scale of the wave propagation kinetics depending on fluid compressibility and solid elastic coefficients.

Références

[1] Barker, A. T., Cai, X.C. 2010 Scalable parallel methods for monolithic coupling in fluid-structure interaction with application to blood flow modeling. *J. Compt. Phys.* **229** 642-659.

[2] Caltagirone, J.P., Vincent, S., Caruyer, C. 2011 A multiphase compressible model for the simulation of multiphase flows. *Comput. Fluid.* **50** 24-34.

[3] Cavagna, L., Quaranta, G., Mantegazza, P. 2007 Application of Navier-Stokes simulations for aeroelastic stability assessment in transonic regime. *Comput. Struct.* **85** 818-862.

[4] Degroote, J. Haelterman, R., Annerel, S., Bruggeman, P., Vierendeels, J. 2010 Performance of partitioned procedures in fluid-structure interaction. *Comput. Struct*. **88** 446-457.

[5] Khadra, K., Angot, P., Parneix, S., Caltagirone, J.P. 2000 Fictitious domain approach for numerical modelling of Navier-Stokes equations. *Int. J. Numer. Meth. Fluid.* **34** 651-684.

[6] Lopez, J., Hernandez, J., Gomez P., Faura F. 2005 An improved PLIC-VOF method for tracking thin fluid structures in incompressible two-phase flows. *J. of Comput. Phys.* **208** 51-74.

[7] Quaini, A., Canic, S., Glowinski, R., Igo, S., Hartley, C.J., Zoghbi, W., Little, S. 2012 Validation of a 3D computational fluid-structure interaction model simulating flow through an elastic aperture, *J. Biomech.* **45** 310-31.